Research Square

Preprints are preliminary reports that have not undergone peer review.
They should not be considered conclusive, used to inform clinical practice,
or referenced by the media as validated information.

Single-Cell and Spatial Transcriptomics Identify CDKN2A as a Ferroptosis-Related Regulator of 5-Fluorouracil Resistance in Colorectal Cancer

Yaoxing Duan
Gansu Provincial People's Hospital
Xiaojiang Bao
Gansu Provincial People's Hospital
Lede Liu
Gansu Provincial People's Hospital
Jingjing Li
Gansu Provincial People's Hospital
Ling Wang
404141809@qq.com
Gansu Provincial People's Hospital

Research Article

Keywords: Colorectal cancer, 5-Fluorouracil resistance, Ferroptosis, CDKN2A, Single-cell transcriptomics

Posted Date: November 20th, 2026

DOI: https://doi.org/10.21203/rs.3.rs-11444282/v1

License: This work is licensed under a Creative Commons Attribution 4.0 International License.
Read Full License

Additional Declarations: No competing interests reported.

Single-Cell and Spatial Transcriptomics Identify CDKN2A as a Ferroptosis-Related Regulator of 5-Fluorouracil Resistance in Colorectal Cancer

Yaoxing Duan[1,], Xiaojiang Bao[1], Lede Liu[1], Jingjing Li[1],Ling Wang[2*]

1. Department of Anorectal Surgery, Gansu Provincial People's Hospital, Lanzhou, Gansu Province 730000, China

2. Department of Pathology, Gansu Provincial People's Hospital, Lanzhou, Gansu Province 730000, China

*Correspondence: Ling Wang; Doctor; Department of Pathology, Gansu Provincial People's Hospital, Lanzhou, Gansu Province 730000, China; Email: 404141809@qq.com

Keywords: Colorectal cancer; 5-Fluorouracil resistance; Ferroptosis; CDKN2A; Single-cell transcriptomics

Abstract

Colorectal cancer (CRC) is a leading cause of cancer-related mortality, and chemotherapy resistance remains a major obstacle to effective treatment. Ferroptosis has emerged as a potential therapeutic vulnerability in drug-resistant tumors, but its role in CRC chemotherapy resistance remains incompletely understood. Here, we integrated bulk transcriptomic, single-cell RNA sequencing, spatial transcriptomic, and experimental analyses to identify ferroptosis-related determinants of chemotherapy resistance in CRC. Transcriptomic analysis identified 28 chemotherapy resistance-related ferroptosis genes. Single-cell analysis showed that malignant epithelial cells had lower Chemotherapy Resistance Ferroptosis Scores (CRFscores) than normal epithelial cells, while CRFscore-low malignant cells exhibited enhanced metabolic activity and tumor-promoting pathway features. CDKN2A emerged as a key candidate associated with unfavorable chemotherapy outcomes, reduced ferroptosis-related activity, and stronger spatial associations with myeloid populations. Functional validation in HCT116/5-FU and HCT8/5-FU cells showed that CDKN2A was upregulated in resistant cells, whereas CDKN2A depletion enhanced 5-FU sensitivity and reduced clonogenic survival. CDKN2A knockdown also increased lipid ROS, intracellular labile iron, and malondialdehyde accumulation, while ferrostatin-1 partially reversed these effects. Moreover, CDKN2A depletion reduced PI3K and AKT phosphorylation and decreased SLC7A11 and GPX4 expression. Collectively, our findings identify CDKN2A as a potential regulator linking ferroptosis resistance to 5-FU resistance in CRC and suggest that

CDKN2A-associated ferroptosis resistance may represent a therapeutic vulnerability for overcoming chemotherapy resistance.

Introduction

Colorectal cancer (CRC) represents a significant global health challenge, being one of the most prevalent malignancies and a leading cause of cancer-related mortality. The disease is characterized by a complex interplay of genetic, environmental, and lifestyle factors, which contribute to its pathogenesis and progression [1-3]. Epidemiological studies indicate that CRC incidence is rising, particularly in younger populations, underscoring the urgent need for effective prevention and treatment strategies. The economic burden of CRC is substantial, encompassing direct medical costs, lost productivity, and the emotional toll on patients and their families [4]. Current treatment modalities primarily include surgical resection, chemotherapy, and targeted therapies [5, 6]; however, the efficacy of these approaches is often compromised by the development of chemotherapy resistance [7], which remains a formidable obstacle in the management of CRC.

Chemotherapy resistance in CRC is a multifaceted phenomenon influenced by various biological mechanisms, including alterations in drug metabolism, enhanced DNA repair capabilities, and evasion of apoptosis. Recent research has highlighted the role of ferroptosis, a regulated form of cell death characterized by iron-dependent lipid peroxidation, in the context of cancer therapy [8]. Ferroptosis has emerged as a potential therapeutic target, as its induction can circumvent resistance mechanisms and promote tumor cell death [9]. However, the relationship between ferroptosis and chemotherapy resistance in CRC is not fully understood, and existing studies have primarily focused on the general mechanisms of ferroptosis without elucidating specific gene interactions that may influence treatment outcomes.

In the realm of molecular biology, several studies have identified key genes associated with ferroptosis, yet the specific contributions of these genes to chemotherapy resistance in CRC remain largely unexplored. For instance, while genes such as GPX4 and SLC7A11 have been implicated in the regulation of ferroptosis [10], their roles in the context of CRC chemotherapy resistance are not well characterized. Furthermore, the interplay between ferroptosis-related genes and the tumor microenvironment, particularly the immune landscape, is an area ripe for

investigation. The immune system plays a critical role in tumor progression and response to therapy [11], and understanding how ferroptosis influences immune cell dynamics could provide valuable insights into enhancing therapeutic efficacy.

In this study, we sought to systematically characterize the relationship between ferroptosis and chemotherapy resistance in CRC and to identify potential molecular regulators underlying this association. We first analyzed transcriptomic data from CRC patients receiving postoperative chemotherapy to identify chemotherapy resistance-related ferroptosis genes. Single-cell RNA sequencing and spatial transcriptomic analyses were subsequently integrated to characterize ferroptosis-related malignant cell states, their biological features, and their spatial relationships with the tumor microenvironment. CDKN2A was identified as a key candidate associated with chemotherapy outcome and reduced ferroptosis-related activity. Finally, its functional role was evaluated in two independent 5-FU-resistant CRC cell models by assessing chemotherapy sensitivity, ferroptosis-related phenotypes, and associated signaling alterations. Through the integration of multi-level transcriptomic analyses and experimental validation, this study provides new insights into the role of CDKN2A-associated ferroptosis resistance in CRC chemotherapy resistance.

Methods

Data resources

High-throughput data were downloaded from the GEO database. GSE106584 contains transcriptomic data from colorectal cancer patients who underwent postoperative chemotherapy, along with their treatment response information [12]. GSE132257 includes single-cell sequencing data for colorectal cancer [13]. Spatial transcriptomics data for colorectal cancer was obtained from GSE225857 [14]. Ferroptosis-related genes were retrieved from the Ferrdb database (zhounan.org/ferrdb) [15].

Differential Expression Analysis

Differential expression analysis was performed using the limma package in R to identify genes associated with chemotherapy resistance in colorectal cancer. The analysis compared patients with no evidence of disease (NED, n=72) to those who died of the disease (DOD, n=56). Genes

with a P-value < 0.05 and an absolute log fold change (logFC) > 0 were considered significant. Genes that intersected with ferroptosis-related genes from FerrDb were selected for further analysis. Differentially expressed genes were visualized using volcano plots and heatmaps.

Identification of Crucial Chemotherapy Resistance-Ferroptosis-related Genes

Key genes associated with chemotherapy resistance were identified through LASSO regression analysis. Gene expression data from TCGA was filtered to retain relevant genes based on prior differential analysis. A LASSO regression model was constructed using the glmnet package, with a binomial family and alpha set to 1 for L1 regularization. Cross-validation (10-fold) was performed to select the optimal lambda value, minimizing deviance. Genes with non-zero coefficients at the optimal lambda were identified as potential resistance-related genes and saved for downstream analysis. Survival analysis of key genes was performed using the K-M plotter (https://kmplot.com/analysis/) website. Pan-cancer analysis and immune infiltration analysis of key genes were conducted using the SangerBox web tool.

Single-Cell Transcriptomic Data Analysis and Malignant Cell Identification

Single-cell transcriptomic data analysis was conducted reveal the mechanisms of chemotherapy resistance-ferroptosis-related genes. The analysis began with quality control and filtering of low-quality cells based on standard metrics on dataset GSE132257. The data was normalized and log-transformed before clustering analysis using Seurat's clustering algorithm, which was based on principal component analysis (PCA) and graph-based methods. Malignant cells were identified with CopyKAT package [16].

Gene Set Scoring in single cell data

Next, we loaded the Chemotherapy Resistance-Ferroptosis-related Genes and calculated a gene score using the AddModuleScore function from Seurat. The specific Chemotherapy Resistance-Ferroptosis-related scores (CRFscore) was added to the Seurat object. We visualized the results using FeaturePlot, VlnPlot, and DotPlot, with VlnPlot providing the distribution of the gene score across different clusters, The distribution of the CRFscore was further analyzed using plot_density of Nebulosa package to examine the correlation between gene scoring and cluster

characteristics.

Cell Cycle Analysis

To perform cell cycle analysis, cell cycle scoring were performed using the S and G2M phase gene lists with CellCycleScoring function. For visualizing cell cycle phase distribution and CRFscore or CDKN2A expression, we used the VlnPlot and DotPlot functions from Seurat. The Phase annotation provided insight into how CRFscore or CDKN2A expression varies across different phases.

Single-cell Cell-Cell Communication Analysis

We performed cell-cell communication analysis using the CellChat package and communication pathways were analyzed using the human CellChat database [17]. Ligand-receptor interactions and over-expressed genes were identified, and communication probabilities were calculated. Results were visualized using heatmaps to show interactions between cell types. Circular network plots were also created to visualize interaction counts and strengths.

Transcription Factor Analysis

For transcription factor (TF) analysis, we utilized the DoRothEA package to analyze the gene expression data and assess the activity of transcription factors across different cell types. First, we subset the data to include only epithelial cells and filtered out undefined gene groups. The DoRothEA regulon for human data was applied to identify transcription factors with high confidence levels. We then ran the VIPER method, which provides an activity score for each transcription factor based on gene expression data, using a scale-based method. These scores were further summarized by cell type to identify the most variable transcription factors across different groups. The final data was visualized using heatmaps to illustrate the variation in transcription factor activity across different cell types and gene sets.

Pseudotime Analysis

To explore the differentiation trajectory of malignant epithelial cells, we performed pseudotime analysis using the Slingshot package [18]. The pseudotime trajectory was inferred using the Slingshot method, where cell clusters were connected along a trajectory, allowing us to examine

the differentiation process of the malignant cells. The pseudotime values were assigned to each cell, enabling the identification of gene expression patterns along the progression.

Metabolism Analysis

For metabolism analysis, we focused on assessing the metabolic activity of epithelial cells, particularly in relation to macromolecular metabolism pathways. The scMetabolism package [19] was applied to evaluate the metabolism activity of individual cells using AUCell-based scoring for KEGG pathways. Pathway scores were extracted, and metabolic activity was compared across different cell groups. Additionally, metabolic signatures were visualized using dot plots, which revealed the specific pathways enriched in different gene groups. This analysis provided insights into the metabolic state of epithelial cells and its association with cellular differentiation and malignancy.

Spaital transcriptomic analysis.

In spatial analysis, RCTD deconvolution technology was initially used to process single-cell data. The spacexr package was used for spatial data processing, defining functions to convert sparse matrices into regular matrices and constructing a spatial RNA object to perform RCTD analysis. The spatial distribution of cell types was visualized using the SpatialFeaturePlot function.

For neighborhood network analysis, the spatial data of the samples were loaded, and the deconvolution matrix was merged with the spatial dataset to extract regions containing the cell types of interest. A K-nearest neighbor network was constructed, calculating the distance between spatial points to create interaction networks between cells. Significant regions with high expression of specific cell types were extracted by adjusting thresholds. The network construction was based on the distances between spatial locations, and the degree matrix was analyzed to assess the connectivity of different spatial points. Ultimately, the networks and their distribution in the spatial images were visualized.

The mistyR analysis is designed to explore spatial interactions in tissue samples, particularly focusing on colocalization of features across different spatial regions (intra, juxta, and para). [20]. Interaction heatmaps and community plots were performed for each spatial view type (intra, juxta, and para). The output provides valuable insights into spatial relationships between features

and allows the identification of key interactions within the tissue. Additionally, the SPOTlight package is used to visualize correlations and interactions between the different spatial features [21].

Gene Set Enrichment Analysis (GSEA)

Gene Set Enrichment Analysis (GSEA) was performed to identify enriched pathways using ranked gene expression data. We used the clusterProfiler package in R and curated gene sets from MSigDB. GSEA was applied to compare different conditions, such as CRFscore high and low malignant cells. Enrichment scores (ES) were calculated for each gene set, and results were filtered based on false discovery rate (FDR).

Cell Culture and Establishment of 5-FU-Resistant CRC Cells

Human colorectal cancer cell lines HCT116 and HCT8 were obtained from Haixing Biosciences (China) and cultured in RPMI-1640 supplemented with 10% fetal bovine serum and 1% penicillin–streptomycin at 37 °C in 5% CO_2. The 5-FU-resistant derivatives HCT116/5-FU and HCT8/5-FU were generated by continuous exposure to gradually increasing concentrations of 5-FU over approximately 10 months. Resistant cells were maintained in medium containing 5 μM 5-FU and cultured in drug-free medium for 48 h before subsequent experiments. All cell lines used in this study were routinely tested for mycoplasma contamination and were confirmed to be mycoplasma-free before use in experiments.

siRNA Transfection and Drug Treatment

Small interfering RNA targeting CDKN2A (siCDKN2A) and negative control siRNA (siCtrl) were purchased from GenePharma (Shanghai, China). The siRNA sequence targeting human CDKN2A (CDKN2A-Homo-448) was 5′-AGUAACCAUGCCCGCAUAGTT-3′ (sense) and 5′-CUAUGCGGGCAUGGUUACUTT-3′ (antisense). Cells were transfected using siRNA-Mate™ transfection reagent (GenePharma) at a final siRNA concentration of 5 nM, and knockdown efficiency was confirmed by Western blotting. For ferroptosis-related experiments, cells were divided into Control, siCtrl, siCDKN2A, siCDKN2A + ferrostatin-1 (Fer-1), and siCtrl + RSL3 groups, with Fer-1 and RSL3 administered at 2 μM for 24 h.

Cell Viability Assay

Cell viability was evaluated using a Cell Counting Kit-8 (CCK-8; Yeasen). Cells were seeded in 96-well plates and treated with increasing concentrations of 5-FU for 48 h, followed by incubation with CCK-8 reagent. Absorbance was measured at 450 nm, and dose–response curves and IC50 values were calculated using nonlinear regression in GraphPad Prism.

Colony Formation Assay

Cells were seeded in six-well plates at a density of 1000 cells per well and cultured under the indicated treatment conditions for approximately 14 days. Colonies were then fixed with 4% paraformaldehyde (PFA), stained with crystal violet, and counted. Colony formation was expressed relative to the corresponding control group.

Quantitative Real-Time PCR

Total RNA was extracted using TRIzol reagent and reverse-transcribed into cDNA using TIANGEN FastKing gDNA Dispelling RT SuperMix kit. Quantitative real-time PCR was performed using SuperReal Color PreMix on a QuantStudio 5 Real-Time PCR System (Applied Biosystems). Relative CDKN2A expression was normalized to GAPDH and calculated using the 2^−ΔΔCt method. The primer sequences were as follows: CDKN2A/p16^INK4A, forward 5′-CCAACGCACCGAATAGTTACG-3′ and reverse 5′-GCGCTGCCCATCATCATG-3′; GAPDH, forward 5′-AGCCACATCGCTCAGACAC-3′ and reverse 5′-GCCCAATACGACCAAATCC-3′, as previously described [22].

Western Blot Analysis

Total cellular proteins were extracted using RIPA buffer containing protease and phosphatase inhibitors. Equal amounts of protein were separated by SDS-PAGE and transferred onto PVDF membranes. After blocking, membranes were incubated with primary antibodies against CDKN2A, PI3K, p-PI3K, AKT, p-AKT, SLC7A11, GPX4, and β-actin, followed by HRP-conjugated secondary antibodies. Protein bands were visualized using enhanced chemiluminescence and quantified using ImageJ, with p-PI3K and p-AKT normalized to total PI3K and AKT, respectively.

C11-BODIPY Lipid Peroxidation Assay

Lipid ROS were assessed using C11-BODIPY 581/591 (Beyotime). Following the indicated treatments, cells were incubated with 2 μM C11-BODIPY 581/591 for 30 min at 37 °C in the dark, washed with PBS, and immediately imaged by fluorescence microscopy. Increased green fluorescence was interpreted as enhanced lipid peroxidation and quantified using ImageJ.

Measurement of the Intracellular Labile Iron Pool

The intracellular labile iron pool was measured using calcein-AM (Beyotime). After treatment, cells were incubated with 2 μM calcein-AM for 30 min at 37 °C in the dark and analyzed by flow cytometry. Because labile intracellular iron quenches calcein fluorescence, reduced fluorescence intensity was interpreted as an increased labile iron pool.

Malondialdehyde Assay

Malondialdehyde (MDA) levels were measured using an Lipid Peroxidation MDA Assay Kit (Beyotime) according to the manufacturer's instructions. Cells were collected after the indicated treatments, lysed, and reacted with the assay reagents. Absorbance was measured at 532 nm, and MDA levels were normalized to total protein concentration.

Statistical Analysis

Statistical analyses were conducted using R version 4.2.2 and GraphPad Prism version 10.1.2 For comparisons between two groups, Student's t-test or the Wilcoxon rank-sum test was used for continuous variables, depending on data distribution. Comparisons among multiple experimental groups were performed using one-way analysis of variance (ANOVA) followed by an appropriate multiple-comparison test, or the Kruskal–Wallis test for non-normally distributed data. For categorical variables, Chi-square tests or Fisher's exact tests were applied. Pearson's or Spearman's correlation coefficients were used to assess correlations, as appropriate. Dose–response curves were fitted using nonlinear regression, and half-maximal inhibitory concentration (IC50) values were calculated using GraphPad Prism. Multiple-testing correction for transcriptomic analyses was performed using the Benjamini–Hochberg method to control the

false discovery rate (FDR). Experimental data are presented as mean ± standard deviation (SD) from at least three independent experiments unless otherwise indicated. All statistical tests were two-tailed, and $P < 0.05$ was considered statistically significant.

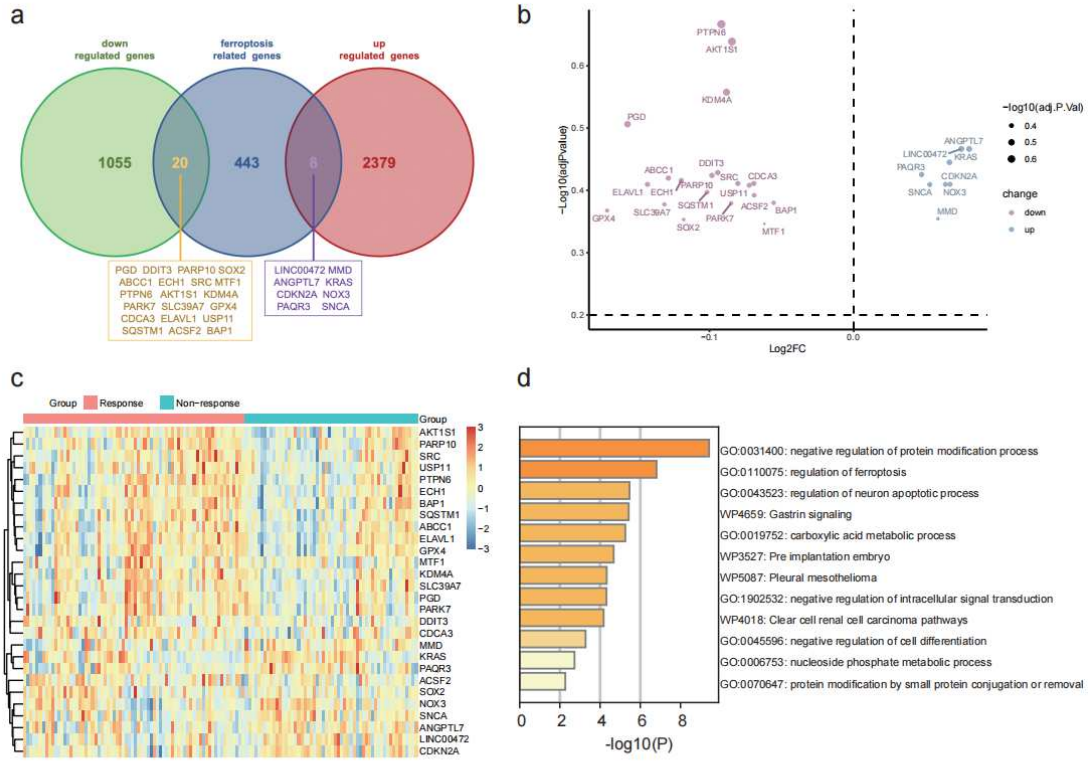


Figure 1. Identification and characterization of chemotherapy resistance-related ferroptosis genes. (a) Venn diagram showing the overlap of upregulated and downregulated genes in colorectal cancer patients with postoperative chemotherapy, stratified by survival status (no evidence of disease (NED) vs. died of disease (DOD)), and 443 ferroptosis-related genes. A total of 28 chemotherapy resistance-related ferroptosis genes were identified. (b) Volcano plot illustrating the differential expression of the 28 genes between the NED and DOD groups, highlighting the upregulated genes (e.g., CDKN2A, NOX3, SNCA) and downregulated genes (e.g., PARK7, SLC39A7, GPX4). (c) Heatmap showing the expression patterns of the identified genes in the NED and DOD groups, with rows representing genes and columns representing samples. (d) Enrichment analysis results from Metascape, highlighting the involvement of these genes in pathways related to ferroptosis, apoptosis, signal transduction, cell differentiation, and metabolism, suggesting their potential influence on chemotherapy drug sensitivity.

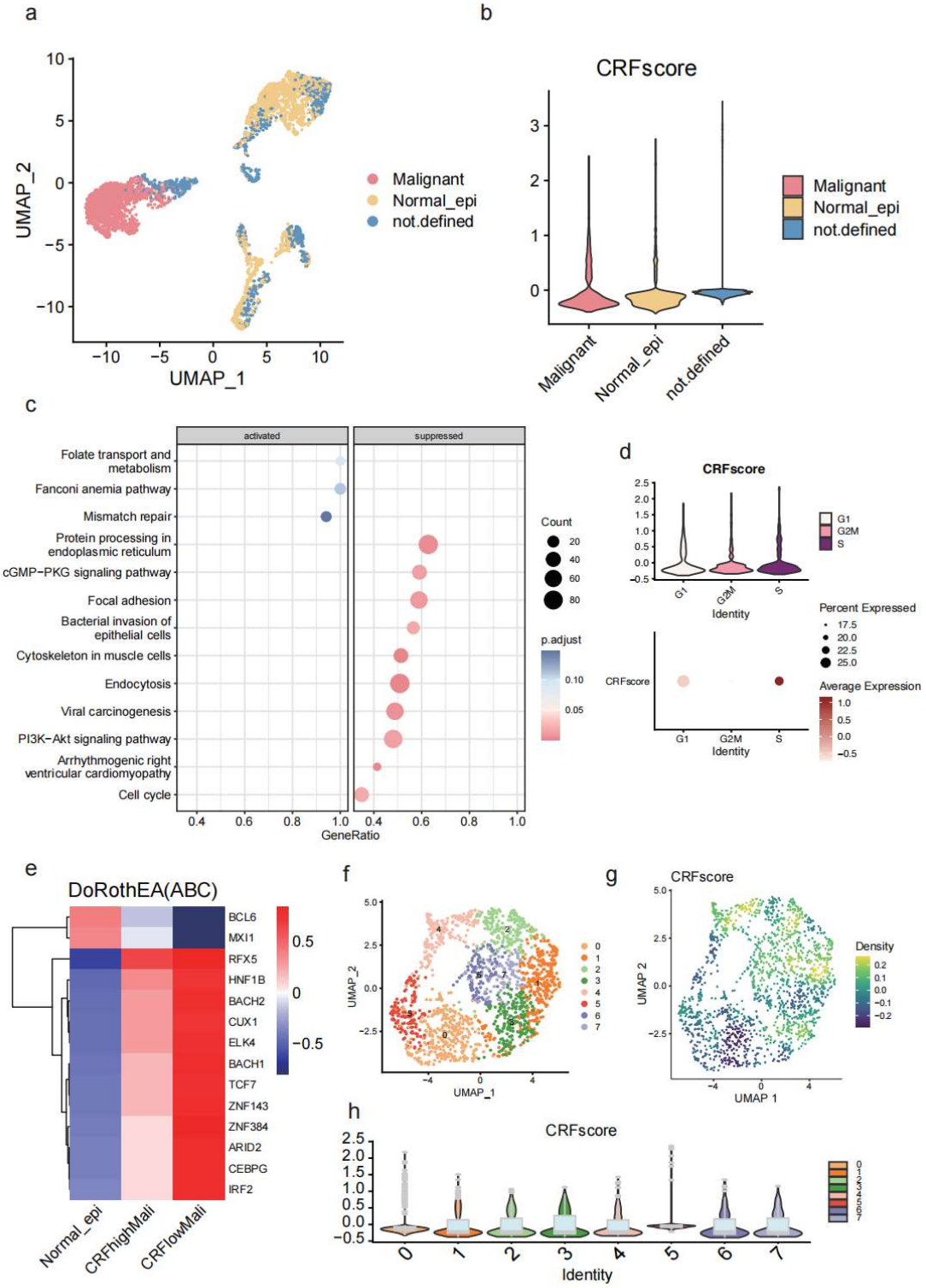


Figure 2. Analysis of chemotherapy resistance-related ferroptosis genes in the tumor microenvironment using single-cell RNA-seq. (a) The predicted benign and malignant epithelial subpopulations using CopyKAT, with scoring of chemotherapy resistance-related ferroptosis genes. (b) Chemotherapy Resistance Ferroptosis Score (CRFscore) comparison between

malignant and normal epithelial cells, showing that malignant cells have a lower CRFscore, suggesting a loss of ferroptotic activity that may contribute to chemotherapy resistance. (c) Differential analysis and Gene Set Enrichment Analysis (GSEA) results based on high and low CRFscore in malignant cells. (d) Cell cycle analysis revealing that cells with high CRFscore are predominantly in the S-phase. (e) Transcription factor analysis indicating that ferroptosis-sensitive tumor cells (high CRFscore) exhibit transcription factor profiles closer to normal cells, while ferroptosis-resistant cells (low CRFscore) show distinct differences. (f-h) Clustering of epithelial cells reveals variability in CRFscore across different subpopulations, with cluster5 exhibiting the highest CRFscore.

Results

Identification of Chemotherapy Resistance-Related Ferroptosis Genes

To identify chemotherapy resistance-related ferroptosis genes, we compared the expression profiles of colorectal cancer patients in the postoperative chemotherapy dataset, stratified by survival status (no evidence of disease (NED), died of the disease (DOD)). This analysis identified 2,379 upregulated genes and 1,055 downregulated genes. By intersecting these genes with 443 ferroptosis-related genes, we found a total of 28 chemotherapy resistance-related ferroptosis genes **(Fig.1a)**. The upregulated genes included CDKN2A, NOX3, and SNCA, while the downregulated genes included PARK7, SLC39A7, and GPX4. We further visualized these gene expression differences between the two groups using volcano plots and heatmaps **(Fig.1b, 1c)**. Additionally, enrichment analysis of these genes using the Metascape website revealed that, in addition to regulating ferroptosis, these genes are involved in pathways related to apoptosis, signal transduction, cell differentiation, and metabolism, suggesting their potential role in influencing chemotherapy drug sensitivity **(Fig.1d)**.

Single-Cell Analysis of Chemotherapy Resistance-Related Ferroptosis Genes

To further explore the role of chemotherapy resistance-related ferroptosis genes in the tumor microenvironment, we analyzed single-cell RNA-seq data from colorectal cancer. Using CopyKAT, we predicted benign and malignant epithelial subpopulations and scored them for chemotherapy resistance-related ferroptosis genes **(Fig. 2a)**. We constructed a Chemotherapy Resistance

Ferroptosis Score (CRFscore). We found that CRFscore was lower in malignant cells compared to normal epithelial cells, suggesting that malignant cells lose some ferroptotic activity, which may contribute to uncontrolled growth and chemotherapy resistance **(Fig. 2b)**. We divided the malignant cells into high and low CRFscore groups and performed differential analysis and GSEA enrichment analysis using FindMarkers **(Fig. S1a)**. We found that high CRFscore suppressed the cell cycle and inhibited the PI3K-Akt signaling pathway, along with the repression of several HALLMARK pathways **(Fig. 2c, Fig. S1b)**. This indicates that ferroptosis itself may inhibit tumor cells and could be associated with chemotherapy sensitivity. Cell cycle analysis showed that cells with high CRFscore were enriched in the S-phase, where cells form chromosomes and divide, making them more susceptible to chemotherapy **(Fig. 2d)**. Transcription factor analysis suggested that ferroptosis-sensitive tumor cells (high CRFscore) have transcription factor features closer to normal cells, while ferroptosis-resistant cells (low CRFscore) showed marked differences from normal cells **(Fig. 2e)**. Further clustering of epithelial cells revealed variability in CRFscore across different subpopulations, with the cluster5 having the highest CRFscore **(Fig. 2f, 2g, 2h)**.

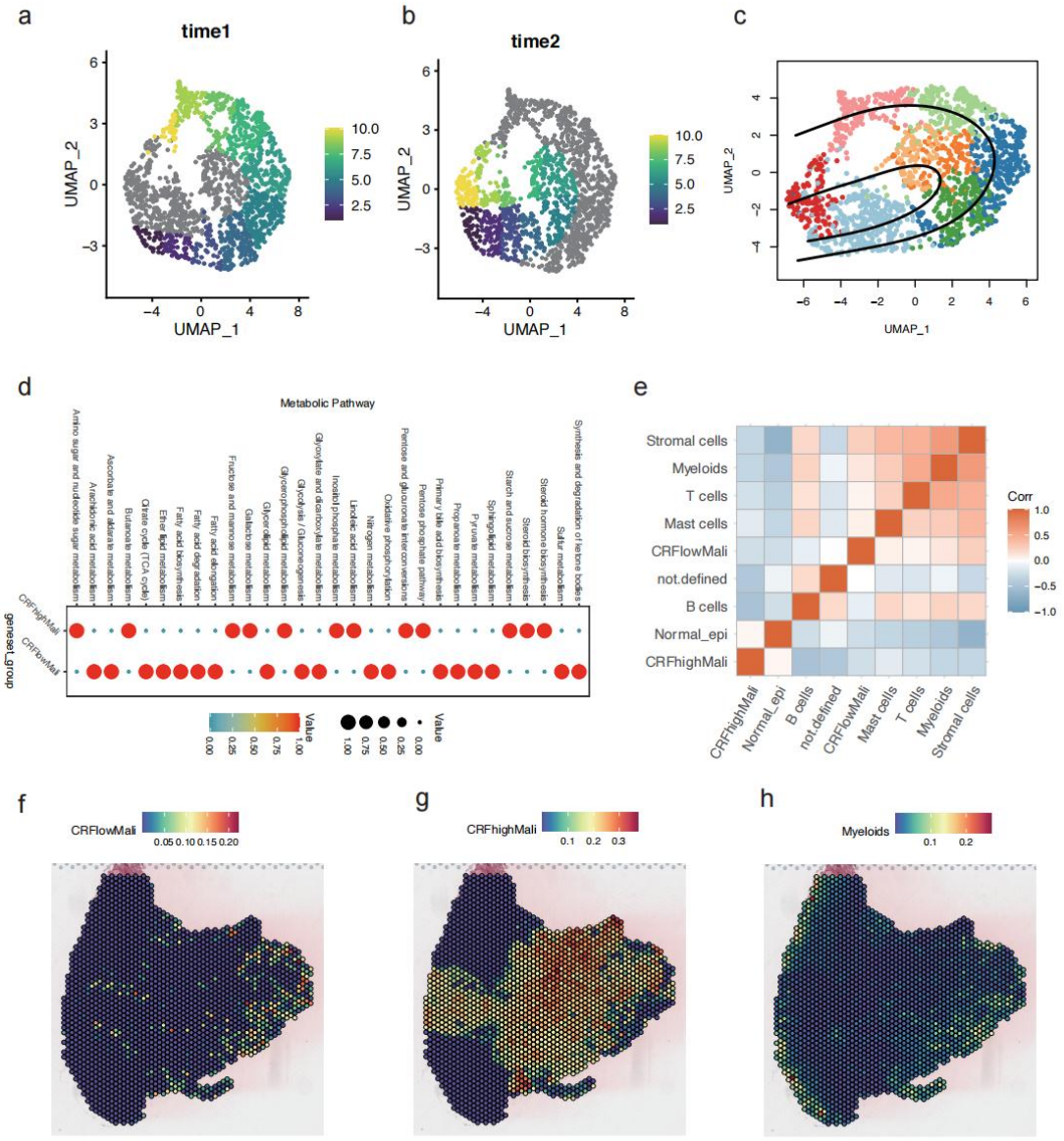


Figure 3. Pseudotime and Spatial Transcriptomics Analysis of Chemotherapy Resistance-Related Ferroptosis Genes. (a-c) Pseudotime analysis of malignant cell subpopulations. (d) Single-cell metabolic analysis of high and low CRFscore tumor cells. (e) Spatial correlation analysis shows that CRFscore-high tumor cells have less influence on surrounding immune cells. (f-h) Spatial feature plot of CRFlowMali CRFhighMali and Myeloid cells.

Pseudotime and Spatial Transcriptomics Analysis of Chemotherapy Resistance-Related Ferroptosis Genes

Pseudotime analysis revealed the developmental trajectory of malignant cell subpopulations,

showing that subgroup 5, which exhibited a high CRFscore, was at the end of the second developmental trajectory, suggesting better differentiation and lower malignancy **(Fig. 3a, 3b, 3c)**. We conducted a single-cell metabolic analysis of high and low CRFscore tumor cells and found that malignant cells with high CRFscore had weaker glycolysis and oxidative phosphorylation capabilities, suggesting lower metabolic activity **(Fig. 3d, Fig. S1c, S1d)**. To further explore their influence on surrounding cells, we performed spatial deconvolution analysis, mapping CRFscore-high and CRFscore-low cells onto colorectal cancer spatial transcriptomics data. Spatial correlation analysis indicated that CRFscore-high tumor cells were less likely to influence surrounding immune cells, while CRFscore-low malignant epithelial cells were more likely to affect other components, such as myeloid cells **(Fig. 3e)**. This suggests that when tumor cells have low ferroptosis scores, they are more likely to induce immune cell reprogramming **(Fig. 3f-3h)**.

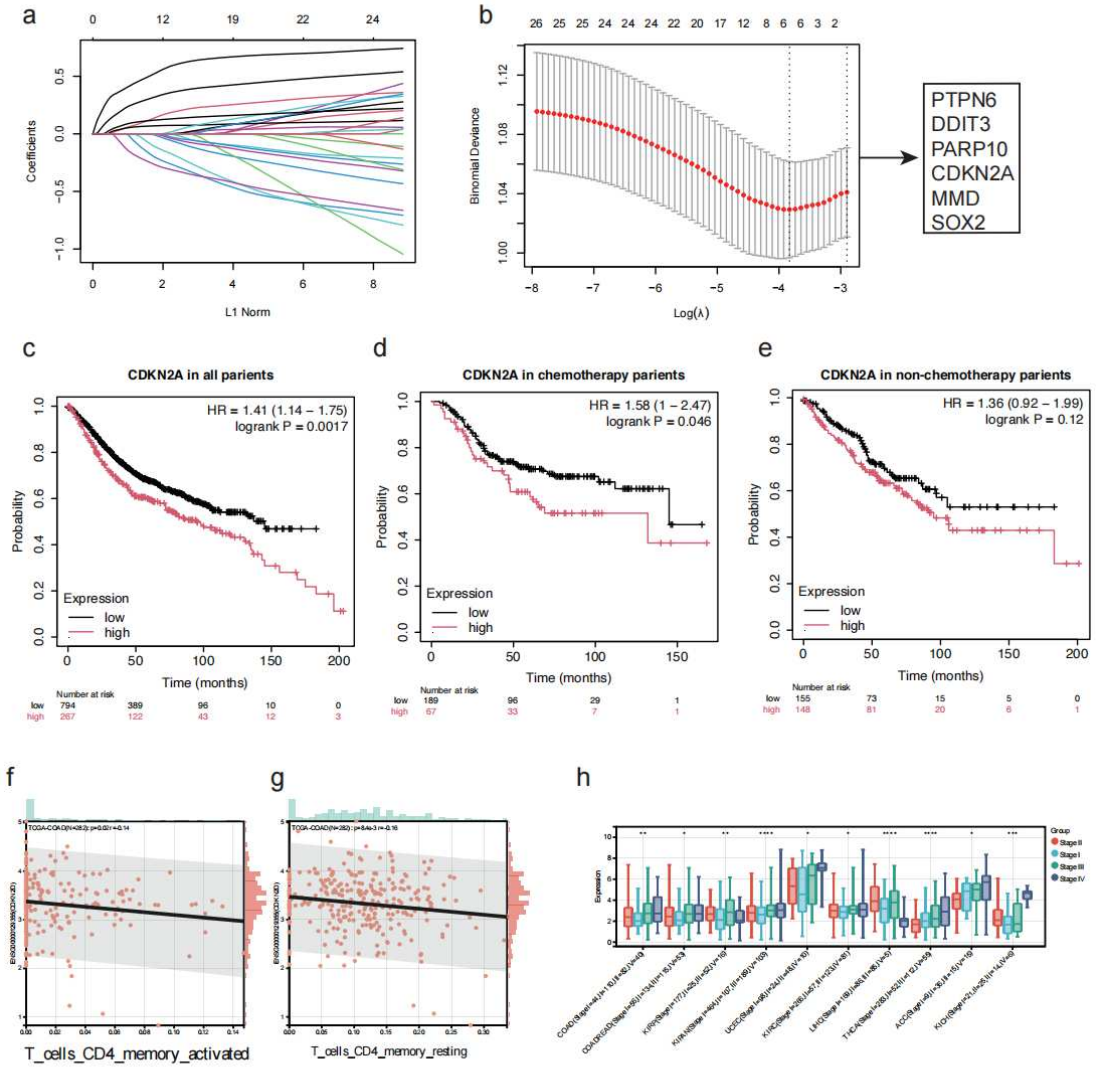


Figure 4. Identification of the Key Chemotherapy Resistance-Related Ferroptosis Gene CDKN2A.

(a, b) LASSO regression analysis of 28 chemotherapy resistance-related ferroptosis genes identified six genes (PTPN6, DDIT3, PARP10, CDKN2A, MMD, SOX2). (c, d, e) Survival analysis shows that CDKN2A is associated with poor overall survival (OS) in both the entire colorectal cancer cohort (c) and in patients receiving chemotherapy (d). No significant difference in OS was observed in patients not receiving chemotherapy (e). (f, g) Associations between CDKN2A expression and CD4+ T-cell infiltration. (h) Pan-cancer analysis of CDKN2A expression across clinical stages.

Identification of the Key Chemotherapy Resistance-Related Ferroptosis Gene CDKN2A

Based on the above analyses, we identified ferroptosis as a protective factor for chemotherapy

sensitivity. We then focused on identifying key risk factors for chemotherapy resistance. We performed LASSO regression on the 28 chemotherapy resistance-related ferroptosis genes and retained 6 genes: PTPN6 (LASSO coef = 0.3738), DDIT3 (LASSO coef = 0.1984), PARP10 (LASSO coef = 0.0382), CDKN2A (LASSO coef = 0.0405), MMD (LASSO coef = -0.0803), and SOX2 (LASSO coef = 0.0697). Among these, only CDKN2A exhibited a positive LASSO coefficient greater than 0 and was found to be upregulated in the chemotherapy-resistant group, suggesting it is a poor prognostic factor and upregulated in the chemotherapy-resistant group **(Fig. 4a, 4b)**. Other genes, such as PTPN6, although exhibiting a positive LASSO coefficient, were found to be downregulated in the chemotherapy-resistant group. Previous studies have indicated that CDKN2A suppresses ferroptosis **(Fig. S2a).** Survival analysis showed that CDKN2A was associated with poor overall survival (OS) in the entire cohort of colorectal cancer patients and in those receiving chemotherapy. However, no significant difference in OS was observed in patients not receiving chemotherapy (P=0.12), suggesting that CDKN2A significantly affects chemotherapy efficacy **(Fig. 4c, 4d, 4e)**. Subgroup analysis revealed that this adverse prognosis was also evident in different cancer stages **(Fig. S2d, 2e)**. Furthermore, immune infiltration analysis indicated that CDKN2A expression was associated with reduced CD4+ T cell infiltration, potentially exacerbating tumor progression **(Fig. 4f, 4g, Fig. S2f, S2g)**. Pan-cancer analysis suggested that CDKN2A is linked to worse clinical staging in multiple cancers **(Fig. 4h, Fig. S2h, S2i)**.

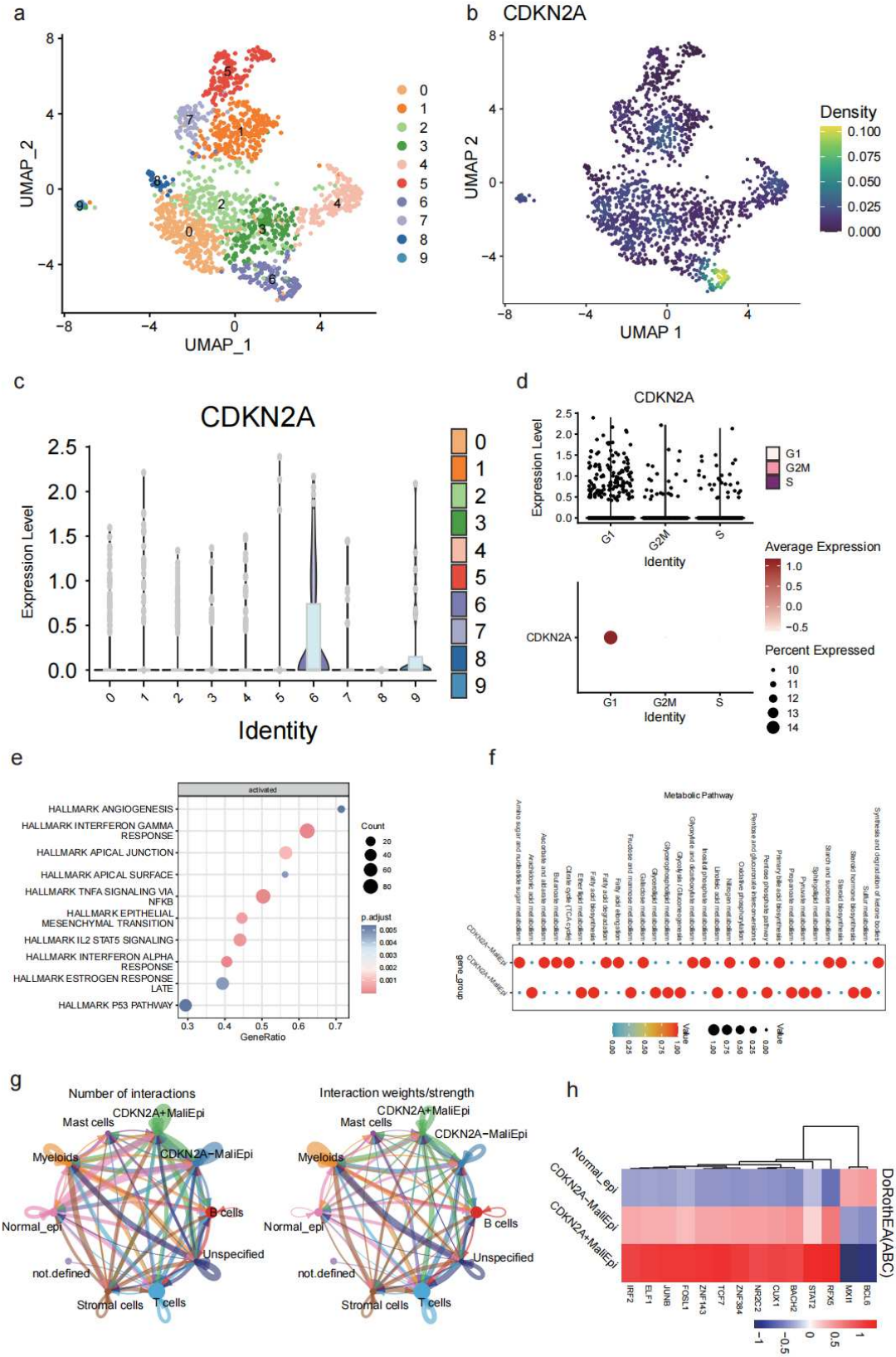


Figure 5. Single-Cell Transcriptomic Analysis of CDKN2A. (a, b, c) Single-cell RNA-seq analysis identified malignant cell subpopulations (0-9), with CDKN2A showing high expression in cell

subgroup 6. (d) Cell cycle analysis reveals that CDKN2A is predominantly expressed in G1-phase cells. (e) Pathway analysis comparing CDKN2A-positive malignant epithelial cells (CDKN2A+MaliEpi) to CDKN2A-negative cells (CDKN2A-MaliEpi). (f) Metabolic analysis shows enhanced glycolysis and increased fatty acid synthesis in CDKN2A-positive malignant cells. (g) Cell communication analysis demonstrates stronger interactions between CDKN2A-positive malignant epithelial cells and other cell types. (h) Transcription factor analysis shows increased transcription factor activity in CDKN2A-positive cells.

Single-Cell Transcriptomic Analysis of CDKN2A

To further understand the function of CDKN2A, we performed single-cell analysis and clustered malignant cells, identifying cell subpopulations 0-9. CDKN2A was highly expressed in cell subgroup 6, suggesting that this subgroup is more likely to be involved in chemotherapy resistance **(Fig. 5a, 5b, 5c)**. Cell cycle analysis indicated that CDKN2A was predominantly expressed in G1-phase cells **(Fig. 5d)**. Pathway analysis of CDKN2A-positive malignant epithelial cells (CDKN2A+MaliEpi) compared to CDKN2A-negative cells (CDKN2A-MaliEpi) revealed activation of pathways associated with angiogenesis and epithelial-mesenchymal transition (EMT), which are associated with tumor progression and aggressive phenotypes **(Fig. 5e)**. Metabolic assessments indicated enhanced glycolysis and increased fatty acid synthesis in CDKN2A-positive malignant cells **(Fig. 5f, Fig. S2b, 2c)**. Cell communication analysis showed that CDKN2A-positive malignant epithelial cells interacted more strongly with other cells **(Fig. 5g)**. Transcription factor analysis revealed increased transcription factor activity in CDKN2A-positive cells, suggesting that CDKN2A, as a ferroptosis inhibitor, contributes to the enhancement of malignant tumor phenotypes **(Fig. 5h)**.

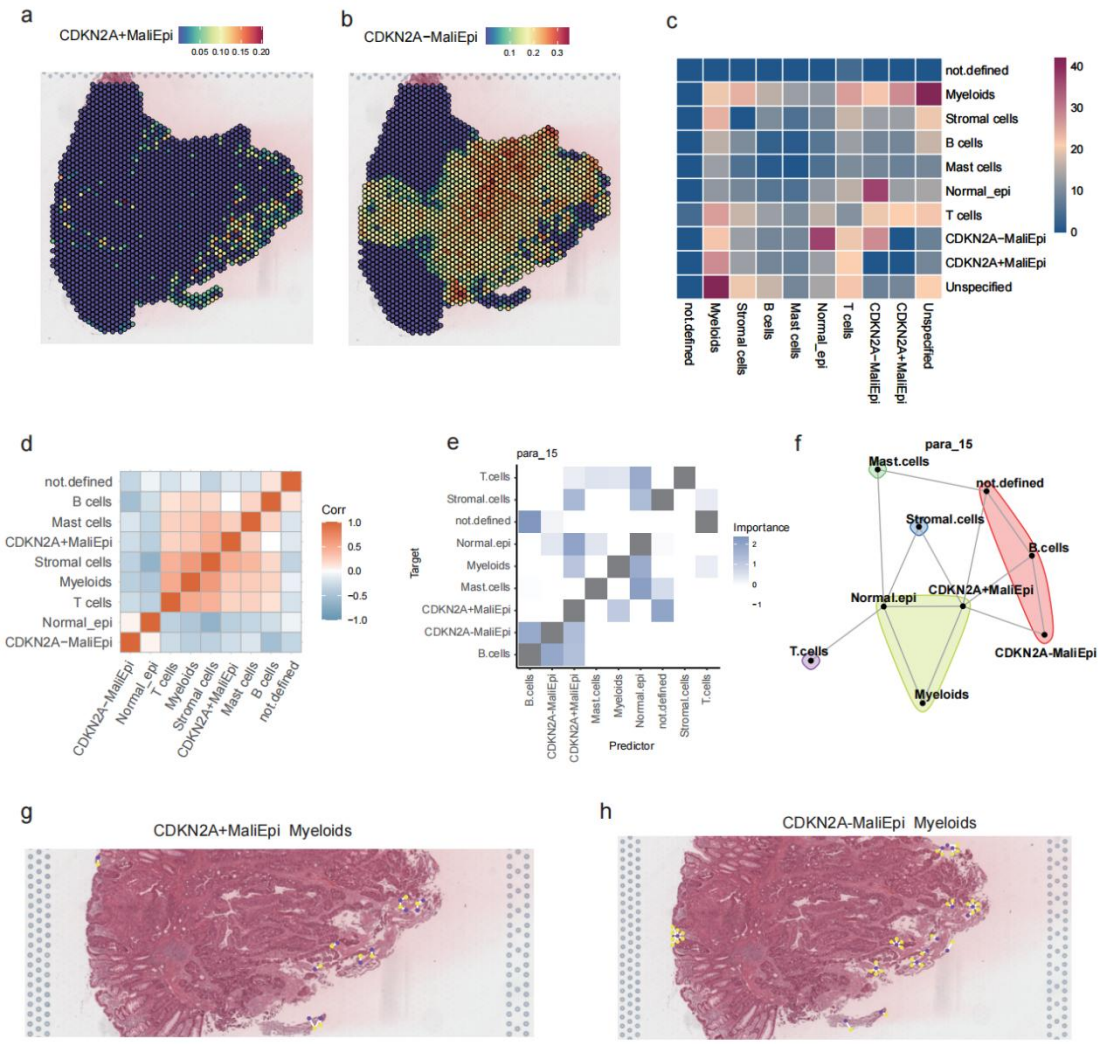


Figure 6. Spatial Transcriptomics Analysis of CDKN2A. (a, b) Spatial feature plot of CDKN2A-positive malignant epithelial cells (CDKN2A+MaliEpi) and CDKN2A-negative cells (CDKN2A-MaliEpi). (c) Cell communication analysis shows that CDKN2A+MaliEpi cells are more likely to interact with myeloid cells. (d) Spatial correlation analysis between CDKN2A+MaliEpi, CDKN2A−MaliEpi, and other cell populations. (e, f) Spatial correlation analysis and MistyR analysis further confirm that CDKN2A+MaliEpi cells exhibit stronger interactions with myeloid cells. (g, h) Spatial network visualization of the associations between myeloid cells and CDKN2A+MaliEpi or CDKN2A−MaliEpi cells, respectively.

Spatial Transcriptomics Analysis of CDKN2A

Spatial transcriptomics analysis of CDKN2A+MaliEpi and CDKN2A-MaliEpi showed that CDKN2A-positive cells and CRFscore-low cells were located in proximity, further supporting the

role of CDKN2A in inhibiting ferroptosis **(Fig. 6a, 6b)**.Cell communication and spatial correlation analyses indicated that CDKN2A+MaliEpi cells were more closely associated with myeloid cells, whereas CDKN2A−MaliEpi cells showed relatively stronger associations with B cells **(Fig. 6c, d)**. mistyR and network analyses further supported the preferential spatial association between CDKN2A+MaliEpi cells and myeloid populations **(Fig. 6e, f)**. Spatial network visualization also showed more prominent CDKN2A+MaliEpi–myeloid associations within tumor regions compared with CDKN2A−MaliEpi cells **(Fig. 6g, h)**. These findings suggest that CDKN2A-positive malignant epithelial cells are characterized by a distinct myeloid-associated spatial microenvironment.

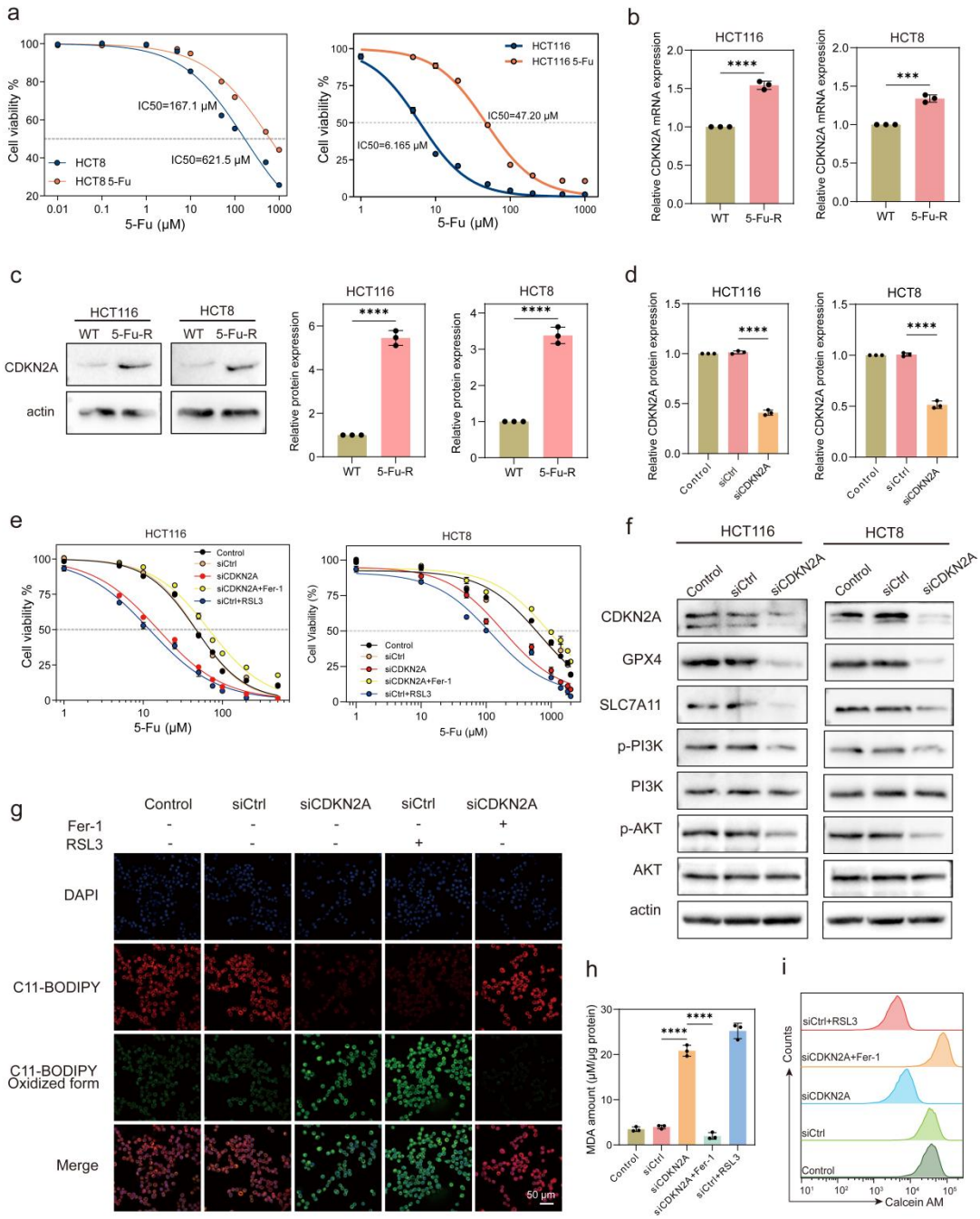


Figure 7. Experimental Validation of CDKN2A in 5-FU Resistance and Ferroptosis. (a) 5-FU dose-response curves of parental and resistant HCT116 and HCT8 cells. (b, c) CDKN2A mRNA and protein expression in parental and resistant cells. (d) Quantification of CDKN2A knockdown efficiency based on the Western blot results shown in (f). (e) 5-FU sensitivity following CDKN2A knockdown and the indicated treatments. (f) Western blot analysis of CDKN2A, PI3K/AKT signaling, SLC7A11, and GPX4. (g) C11-BODIPY fluorescence analysis of lipid peroxidation in HCT116 cells. (h) Intracellular MDA levels in HCT116 cells. (i) Flow cytometric analysis of the intracellular labile iron pool in HCT116 cells. (n = 3, mean ± SD; *P < 0.05, **P < 0.01, ***P < 0.001, ****P < 0.0001).

CDKN2A Depletion Enhances 5-FU Sensitivity and Ferroptosis in Resistant Colorectal Cancer Cells

To experimentally validate the association between CDKN2A and acquired 5-FU resistance, we generated two 5-FU-resistant CRC cell derivatives, HCT116/5-FU and HCT8/5-FU, from their respective parental cell lines. Both resistant derivatives exhibited markedly reduced sensitivity to 5-FU, as indicated by substantially higher IC50 values than those of their corresponding parental cells **(Fig. 7a)**. Consistently, colony formation assays further confirmed the resistant phenotype under 5-FU exposure **(Fig. S3a)**. CDKN2A expression was subsequently examined in the parental and resistant cells. Both qPCR and Western blot analyses showed elevated CDKN2A expression in HCT116/5-FU and HCT8/5-FU cells compared with their parental counterparts **(Fig. 7b, 7c)**, consistent with our bioinformatic findings.

CDKN2A knockdown efficiency was confirmed by Western blotting in both HCT116/5-FU and HCT8/5-FU cells **(Fig. 7d, 7f)**. CDKN2A depletion subsequently increased the sensitivity of resistant CRC cells to 5-FU and reduced colony formation **(Fig. 7e, Fig. S3c)**. Notably, Fer-1 partially reversed these effects, whereas RSL3 produced a similar growth-inhibitory phenotype, suggesting the involvement of ferroptosis. Consistently, CDKN2A knockdown increased C11-BODIPY oxidation, intracellular labile iron levels, and MDA accumulation in HCT116/5-FU cells, while Fer-1 attenuated lipid peroxidation **(Fig. 7g-i)**. These findings indicate that CDKN2A depletion enhances ferroptotic susceptibility and partially restores 5-FU sensitivity in resistant CRC cells.

Our single-cell analysis showed that increased ferroptosis-related activity was associated with suppression of PI3K/AKT signaling. Consistent with this observation, CDKN2A depletion reduced PI3K and AKT phosphorylation and decreased SLC7A11 and GPX4 expression **(Fig. 7f, Fig. S3b)**. Together, these results suggest that CDKN2A contributes to 5-FU resistance by maintaining a ferroptosis-resistant state, potentially associated with PI3K/AKT signaling and the SLC7A11/GPX4 ferroptosis-defense axis.

Discussion

Colorectal cancer (CRC) remains a major global health challenge and one of the leading causes of cancer-related mortality [23]. The development of chemotherapy resistance further limits treatment efficacy and contributes to unfavorable clinical outcomes [24]. In this study, we integrated transcriptomic, single-cell, spatial transcriptomic, and experimental analyses to investigate the relationship between ferroptosis and chemotherapy resistance in CRC. We identified a distinct ferroptosis-related state in malignant cells and further highlighted CDKN2A as a key chemotherapy resistance-related ferroptosis gene. Importantly, functional experiments in two 5-FU-resistant CRC cell models supported the role of CDKN2A in maintaining both chemotherapy resistance and reduced ferroptotic susceptibility.

Our analyses first revealed a close association between ferroptosis-related activity and malignant cellular states. Malignant epithelial cells exhibited lower Chemotherapy Resistance Ferroptosis Scores (CRFscores) than normal epithelial cells, while CRFscore-low malignant cells showed stronger glycolytic and oxidative phosphorylation activity. In contrast, higher ferroptosis-related activity was associated with suppression of several tumor-promoting pathways, including PI3K/AKT signaling. These findings suggest that reduced ferroptosis-related activity may provide malignant cells with a survival advantage and coexist with metabolic adaptations that facilitate tumor progression and chemotherapy resistance. Thus, ferroptosis resistance may represent an important component of the resistant phenotype rather than an isolated alteration in individual ferroptosis-related genes.

Among the identified genes, CDKN2A emerged as a particularly important candidate. CDKN2A is widely recognized for its involvement in cell-cycle regulation and other fundamental cellular processes [25, 26]. Recent studies have further demonstrated that CDKN2A can participate in

ferroptosis regulation, although its effects appear to depend on the cellular context [27, 28]. Consistent with these reports, CDKN2A-positive malignant cells in our single-cell analysis exhibited lower ferroptosis-related activity together with enhanced glycolytic and lipid metabolic features. Moreover, CDKN2A was associated with unfavorable prognosis in patients receiving chemotherapy, whereas this association was not evident in patients without chemotherapy. These observations suggested that CDKN2A may be particularly relevant to the adaptation of CRC cells to chemotherapeutic stress.

Importantly, our experimental findings further strengthened this association. CDKN2A expression was elevated in both HCT116/5-FU and HCT8/5-FU cells compared with their corresponding parental cells, consistent with the chemotherapy-resistant phenotype identified in our transcriptomic analyses. More importantly, CDKN2A depletion enhanced 5-FU sensitivity and reduced clonogenic survival in both resistant cell lines. These findings suggest that CDKN2A is not merely associated with chemotherapy resistance but functionally contributes to the maintenance of acquired 5-FU resistance. The use of two independent resistant CRC cell models further supports the biological relevance of this finding.

The effects of CDKN2A depletion were closely associated with ferroptotic susceptibility. Ferroptosis is characterized by iron-dependent lipid peroxidation, and GPX4 plays a critical role in limiting the accumulation of toxic lipid peroxides [29, 30]. In our experiments, CDKN2A depletion increased C11-BODIPY oxidation, intracellular labile iron, and MDA accumulation. Moreover, ferrostatin-1 partially reversed lipid peroxidation and rescued the growth-inhibitory effects induced by CDKN2A depletion, whereas RSL3 produced a similar ferroptosis-associated phenotype in control cells. These biochemical and pharmacological findings complement our single-cell observation that CDKN2A-positive malignant cells exhibit a relatively ferroptosis-resistant state. Together with previous reports linking CDKN2A to ferroptosis regulation [27, 28], our results suggest that elevated CDKN2A may contribute to 5-FU resistance, at least in part, by maintaining cellular resistance to ferroptotic stress.

Our experimental results also provided molecular support for the pathway alterations predicted by the single-cell analysis. Higher ferroptosis-related activity was associated with suppression of PI3K/AKT signaling, whereas CDKN2A depletion reduced PI3K and AKT phosphorylation and decreased SLC7A11 and GPX4 expression. The SLC7A11/GPX4 system constitutes an important

defense mechanism against ferroptotic lipid peroxidation [29, 31]. Therefore, suppression of PI3K/AKT signaling and reduction of SLC7A11/GPX4 expression provide a plausible explanation for the enhanced lipid peroxidation observed following CDKN2A depletion. These findings highlight a potential connection between CDKN2A, PI3K/AKT signaling, and ferroptosis resistance. Nevertheless, pathway-specific rescue experiments are required to establish whether PI3K/AKT signaling directly mediates the effects of CDKN2A on the SLC7A11/GPX4 axis and 5-FU resistance.

Beyond the intrinsic ferroptosis-resistant phenotype of malignant cells, our study also revealed a potential relationship between CDKN2A and the tumor immune microenvironment. Single-cell RNA sequencing enabled us to characterize the heterogeneity of malignant cellular states at high resolution [32], while spatial transcriptomics further revealed that CDKN2A-positive malignant cells preferentially interacted with myeloid populations [33]. Higher CDKN2A expression was also associated with reduced CD4+ T-cell infiltration. These findings suggest that CDKN2A-associated malignant states may involve both intrinsic ferroptosis resistance and distinct tumor–immune interactions. However, the current spatial findings remain correlative, and our in vitro experiments did not directly investigate immune-cell responses. Further studies are therefore required to determine whether CDKN2A-dependent ferroptosis resistance contributes to myeloid-cell reprogramming or other changes in the immune microenvironment.

A major strength of this study lies in the integration of multiple complementary approaches. Transcriptomic analysis identified chemotherapy resistance-related ferroptosis genes at the patient level, single-cell analysis resolved their heterogeneous distribution and biological states [29], and spatial transcriptomics characterized their relationships with the surrounding microenvironment [30]. These computational findings were subsequently supported by functional experiments in two independent 5-FU-resistant CRC models. The consistency between clinical associations, single-cell phenotypes, pathway predictions, and experimental observations strengthens the evidence linking CDKN2A to ferroptosis-associated chemotherapy resistance.

Several limitations should nevertheless be acknowledged. First, the initial identification of chemotherapy resistance-related genes was based on a specific postoperative chemotherapy cohort, and additional independent cohorts are required to validate the generalizability of these findings. Second, although CDKN2A was functionally validated in two 5-FU-resistant CRC cell models, in vivo and clinical validation remains necessary to determine its therapeutic potential.

Third, although PI3K/AKT signaling and the SLC7A11/GPX4 axis were altered following CDKN2A depletion, pathway-specific rescue experiments were not performed, and the precise causal relationship remains to be established. Finally, the spatial association between CDKN2A-positive malignant cells and immune populations requires further functional validation.

In conclusion, our integrated transcriptomic and experimental analyses identify CDKN2A as a potential functional regulator linking ferroptosis resistance to chemotherapy resistance in CRC. Single-cell and spatial transcriptomic analyses revealed that CDKN2A-positive malignant cells exhibited reduced ferroptosis-related activity, enhanced metabolic characteristics, and distinct associations with the tumor microenvironment. Consistent with these computational findings, CDKN2A was upregulated in 5-FU-resistant CRC cells, whereas its depletion enhanced 5-FU sensitivity and ferroptotic susceptibility, accompanied by increased lipid peroxidation and reduced PI3K/AKT activation and SLC7A11/GPX4 expression. Collectively, these findings support CDKN2A-associated ferroptosis resistance as a potential therapeutic vulnerability in 5-FU-resistant CRC and provide a rationale for further investigation of CDKN2A-directed strategies to improve chemotherapy response.

Clinical trial number

Not applicable.

Ethics approval and consent to participate

This study exclusively analyzed publicly available genomic datasets and conducted in vitro experiments using established cell lines. No human clinical specimens or direct human-participant studies were involved. Therefore, ethics approval and consent to participate were not applicable.

Consent for publication

Not Applicable.

Declaration of competing interest

There are no financial or personal relationships with any commercial entities or organizations

that could be perceived as influencing the study's content, results, interpretation, or conclusions.

Data availability

All transcriptomic, single-cell RNA-seq and spatial transcriptomic datasets analysed in this study were retrieved from public repositories: GSE106584, GSE132257 and GSE225857 from the Gene Expression Omnibus (GEO) database. Ferroptosis-related genes were obtained from the FerrDb database. No new raw sequencing data were generated for this study. Further information supporting the findings of this study is available within the article and its supplementary materials.

Author contributions

Yaoxing Duan: Writing—original draft, Validation, Software, Methodology. Xiaojiang Bao: Validation, Resources, Data curation. Lede Liu: Validation, Resources, Data curation. Jingjing Li: Validation, Resources, Data curation. Ling Wang: Writing—review and editing.

Acknowledgements

This work was supported by the Natural Science Foundation of Gansu Province (Grant No. 25JRRA303), the Special Fund for Natural Sciences Research of Gansu Provincial Science and Technology Plan (Grant No. 26JRRA730), and the institutional research project of Gansu Provincial People's Hospital (Grant No. 24GSSYD-1).

1. Dekker E, Tanis PJ, Vleugels JLA, Kasi PM, Wallace MB: **Colorectal cancer**. *Lancet* 2019, **394**(10207):1467-1480.
2. Kityo A, Lee SA: **Triglyceride-Glucose Index, Modifiable Lifestyle, and Risk of Colorectal Cancer: A Prospective Analysis of the Korean Genome and Epidemiology Study**. *J Epidemiol Glob Health* 2024, **14**(3):1249-1256.
3. Scheurlen KM, Billeter AT, O'Brien SJ, Galandiuk S: **Metabolic dysfunction and early-onset colorectal cancer - how macrophages build the bridge**. *Cancer Med* 2020, **9**(18):6679-6693.
4. Alefan Q, Malhees R, Mhaidat N: **Direct medical cost associated with colorectal cancer in north of Jordan**. *Curr Probl Cancer* 2017, **41**(5):371-381.

5. Strickler JH, Yoshino T, Graham RP, Siena S, Bekaii-Saab T: **Diagnosis and Treatment of ERBB2-Positive Metastatic Colorectal Cancer: A Review**. *JAMA Oncol* 2022, **8**(5):760-769.

6. Biller LH, Schrag D: **Diagnosis and Treatment of Metastatic Colorectal Cancer: A Review**. *JAMA* 2021, **325**(7):669-685.

7. Bukowski K, Kciuk M, Kontek R: **Mechanisms of Multidrug Resistance in Cancer Chemotherapy**. *Int J Mol Sci* 2020, **21**(9).

8. Zhao H, Xu Y, Shang H: **Ferroptosis: A New Promising Target for Ovarian Cancer Therapy**. *Int J Med Sci* 2022, **19**(13):1847-1855.

9. Tang Z, Huang Z, Huang Y, Chen Y, Huang M, Liu H, Ye QA, Zhao J, Jia B: **Ferroptosis: The Silver Lining of Cancer Therapy**. *Front Cell Dev Biol* 2021, **9**:765859.

10. Wang W, Zhao X, Zhou J, Li H: **A novel antitumor mechanism of triptonide in colorectal cancer: inducing ferroptosis via the SLC7A11/GPX4 axis**. *Funct Integr Genomics* 2024, **24**(4):126.

11. Wu Z, Li S, Zhu X: **The Mechanism of Stimulating and Mobilizing the Immune System Enhancing the Anti-Tumor Immunity**. *Front Immunol* 2021, **12**:682435.

12. Zhu J, Deane NG, Lewis KB, Padmanabhan C, Washington MK, Ciombor KK, Timmers C, Goldberg RM, Beauchamp RD, Chen X: **Evaluation of frozen tissue-derived prognostic gene expression signatures in FFPE colorectal cancer samples**. *Sci Rep* 2016, **6**:33273.

13. Lee HO, Hong Y, Etlioglu HE, Cho YB, Pomella V, Van den Bosch B, Vanhecke J, Verbandt S, Hong H, Min JW *et al*: **Lineage-dependent gene expression programs influence the immune landscape of colorectal cancer**. *Nat Genet* 2020, **52**(6):594-603.

14. Wang F, Long J, Li L, Wu ZX, Da TT, Wang XQ, Huang C, Jiang YH, Yao XQ, Ma HQ *et al*: **Single-cell and spatial transcriptome analysis reveals the cellular heterogeneity of liver metastatic colorectal cancer**. *Sci Adv* 2023, **9**(24):eadf5464.

15. Zhou N, Yuan X, Du Q, Zhang Z, Shi X, Bao J, Ning Y, Peng L: **FerrDb V2: update of the manually curated database of ferroptosis regulators and ferroptosis-disease associations**. *Nucleic Acids Res* 2023, **51**(D1):D571-D582.

16. Gao R, Bai S, Henderson YC, Lin Y, Schalck A, Yan Y, Kumar T, Hu M, Sei E, Davis A *et al*: **Delineating copy number and clonal substructure in human tumors from single-cell transcriptomes**. *Nat Biotechnol* 2021, **39**(5):599-608.

17. Jin S, Guerrero-Juarez CF, Zhang L, Chang I, Ramos R, Kuan CH, Myung P, Plikus MV, Nie Q: **Inference and analysis of cell-cell communication using CellChat**. *Nat Commun* 2021, **12**(1):1088.

18. Street K, Risso D, Fletcher RB, Das D, Ngai J, Yosef N, Purdom E, Dudoit S: **Slingshot: cell lineage and pseudotime inference for single-cell transcriptomics**. *BMC Genomics* 2018, **19**(1):477.

19. Wu Y, Yang S, Ma J, Chen Z, Song G, Rao D, Cheng Y, Huang S, Liu Y, Jiang S *et al*: **Spatiotemporal Immune Landscape of Colorectal Cancer Liver Metastasis at Single-Cell Level**. *Cancer Discov* 2022, **12**(1):134-153.

20. Tanevski J, Flores ROR, Gabor A, Schapiro D, Saez-Rodriguez J: **Explainable multiview framework for dissecting spatial relationships from highly multiplexed data**. *Genome Biol* 2022, **23**(1):97.

21. Elosua-Bayes M, Nieto P, Mereu E, Gut I, Heyn H: **SPOTlight: seeded NMF regression to deconvolute spatial transcriptomics spots with single-cell transcriptomes**. *Nucleic Acids Res* 2021, **49**(9):e50.

22. Yamauchi S, Sugiura Y, Yamaguchi J, Zhou X, Takenaka S, Odawara T, Fukaya S, Fujisawa T, Naguro I, Uchiyama Y et al: **Mitochondrial fatty acid oxidation drives senescence**. Sci Adv 2024, **10**(43):eado5887.

23. Zhao K, Li H, Zhang B, Pang W, Yan S, Zhao X, Liu X, Wang W, Han Q, Yao Y *et al*: **Factors influencing advanced colorectal neoplasm anatomic site distribution in China: An epidemiological study based on colorectal cancer screening data**. *Cancer Med* 2023, **12**(24):22252-22262.

24. Deo SVS, Kumar S, Bhoriwal S, Shukla NK, Sharma A, Thulkar S, Das P, Bhagat P, Dhall K, Pathy S *et al*: **Colorectal Cancers in Low- and Middle-Income Countries-Demographic Pattern and Clinical Profile of 970 Patients Treated at a Tertiary Care Cancer Center in India**. *JCO Glob Oncol* 2021, **7**:1110-1115.

25. Sato K, Kusama Y, Tategu M, Yoshida K: **FBXL16 is a novel E2F1-regulated gene commonly upregulated in p16INK4A- and p14ARF-silenced HeLa cells**. *Int J Oncol* 2010, **36**(2):479-490.

26. Bayoglu B, Arslan C, Gode S, Kaya Dagistanli F, Arapi B, Burc Deser S, Dirican A, Cengiz M: **The severity of internal carotid artery stenosis is associated with the cyclin-dependent kinase**

inhibitor 2A gene expression. *J Atheroscler Thromb* 2014, **21**(7):659-671.

27. Yong X, Zhang Y, Tang H, Hu H, Song R, Wu Q: **CDKN2A inhibited ferroptosis through activating JAK2/STAT3 pathway to modulate cisplatin resistance in cervical squamous cell carcinoma**. *Anticancer Drugs* 2024, **35**(8):698-708.

28. Minami JK, Morrow D, Bayley NA, Fernandez EG, Salinas JJ, Tse C, Zhu H, Su B, Plawat R, Jones A *et al*: **CDKN2A deletion remodels lipid metabolism to prime glioblastoma for ferroptosis**. *Cancer Cell* 2023, **41**(6):1048-1060 e1049.

29. Feng H, Stockwell BR: **Unsolved mysteries: How does lipid peroxidation cause ferroptosis?** *PLoS Biol* 2018, **16**(5):e2006203.

30. Dixon SJ, Olzmann JA: **The cell biology of ferroptosis**. Nat Rev Mol Cell Biol 2024, **25**(6):424-442.

31. Qiao Y, Su M, Zhao H, Liu H, Wang C, Dai X, Liu L, Liu G, Sun H, Sun M et al: **Targeting FTO induces colorectal cancer ferroptotic cell death by decreasing SLC7A11/GPX4 expression**. J Exp Clin Cancer Res 2024, **43**(1):108.

32. Choi YH, Kim JK: **Dissecting Cellular Heterogeneity Using Single-Cell RNA Sequencing**. *Mol Cells* 2019, **42**(3):189-199.

33. Ma Y, Yi C, Cai N, Chen J: **Integration of single-cell and spatial transcriptome sequencing identifies CDKN2A as a senescent biomarker in endothelial cells implicating hepatocellular carcinoma malignancy**. *J Cancer Res Clin Oncol* 2024, **150**(11):487.

Supplementary Files

This is a list of supplementary files associated with this preprint. Click to download.

- Supplementary.docx